ACADEMIC PRESS

Available online at www.sciencedirect.com

SCIENCE DIRECT®

Journal of Computational Physics 186 (2003) 279–294

JOURNAL OF COMPUTATIONAL PHYSICS

www.elsevier.com/locate/jcp

ISOD – an anisotropic isovalue-oriented diffusion artificial viscosity for the Euler and Navier–Stokes equations

L. Remaki *, H. Beaugendre, W.G. Habashi

CFD Laboratory, McGill University, 688 Sherbrooke Street West Montreal, Quebec, Canada H3A 2S6

Received 8 October 2002; received in revised form 23 January 2003; accepted 28 January 2003

Abstract

This paper introduces a generic artificial viscosity method based on diffusing along iso-values (curves in 2D and surfaces in 3D). The construction and a study of properties of the method are presented. Application to FEM for the Euler and Navier–Stokes equations is established. The performance of the proposed method is demonstrated through numerical tests and comparison to other classical methods.

Keywords: Artificial viscosity; Dissipation; Diffusion; Upwinding; Anisotropy; Euler; Navier–Stokes; FEM; Iso-values; Numerical methods

1. Introduction

Numerical instability is one of the most serious problems encountered when dealing with the discretization of PDEs, especially convection type and fluid flow problems. These undesired but inherent numerical oscillations are present in finite difference [1], finite element [2,3], finite volume methods [4], as well as meshless procedures [5,6]. A plethora of methods have been proposed to overcome oscillations and odd-even decoupling of the Euler and Navier–Stokes equations, among them the classical upwind methods (CU) [1,2,7,8], the Streamline Upwind methods (SU) [9], and the Streamline Upwind Petrov–Galerkin (SUPG) methods [9]. The challenge is to enhance the stability of a scheme without smearing discontinuities (such as shocks) or diffusing boundary layers. These methods are based on adding artificial diffusion via an operator, or equivalently by an appropriate change of weighting functions, a useful strategy to preserve the consistency of the scheme at each time step and not only at the limit state. Regardless of the manner in which artificial viscosity is introduced, the main distinction between the

* Corresponding author. Tel.: +1-514-398-1710; fax: +1-514-398-8454.
E-mail addresses: lakhdar@cfdlab.mcgill.ca (L. Remaki), heloise@cfdlab.mcgill.ca (H. Beaugendre), wagdi.habashi@mcgill.ca (W.G. Habashi).

0021-9991/03/$ - see front matter
doi:10.1016/S0021-9991(03)00066-4

methods is in the way that the diffusion is oriented. For instance, CU diffuses in all directions, and hence introduces excessive diffusion perpendicular to the flow direction. SU and SUPG methods overcome this shortcoming, as the diffusion is made to act only in the streamline or flow direction. The original version of SUPG method suffered some instabilities when dealing with shocks, and a "discontinuity-capturing operator" was added to establish more control in the solution gradient direction. However, since streamlines are usually perpendicular to shocks, this method smears the discontinuities, if optimality of the diffusion amplitude is not reached.

In summary, one could group methods into two categories: directional and non-directional diffusion methods. To determine the optimal value of the diffusion is a very hard task and unfortunately this is necessary to obtain accurate results if the diffusion is not correctly oriented like in SU/SUPG methods where, as mentioned above, the streamlines (the direction of the diffusion) cross the discontinuities. Moreover, the diffusion values are specific to each problem. To avoid smearing discontinuities and boundary layers by excessive values of diffusion, a method must diffuse tangentially to discontinuities and boundary layers. This motivates our choice to take iso-value surfaces (or curves in 2D) as a direction of diffusion since iso-values are tangent to the shock direction and to boundary layers. Therefore, the smoothing effect along iso-values ensures the stability of the numerical scheme, while avoiding the negative or cross-diffusion effects of classical artificial viscosity methods.

This paper is divided in the following manner; in Section 2 the construction and study of some properties of the ISOD operator are developed. In Section 3 an application to FEM for the Euler and Navier–Stokes equations, using P^1-elements, is studied. Through numerical tests, the effectiveness of the new method is demonstrated and comparisons to other methods are shown in Section 4. We conclude in Section 5.

2. The isovalue-oriented diffusion artificial viscosity model (ISOD): construction and some properties

In this section we first give a definition of the proposed isovalue-oriented diffusion operator, referring to it by Δ_{isod}. We then give an analytical expression of the operator. We finally prove a lemma and a proposition that justify the label "iso-values" oriented diffusion.

Definition 2.1. Let Q be a C^1 given scalar function defined on an open set Ω of $\Re^3$, we define the iso-values oriented diffusion operator $\Delta_{\text{isod}}Q$ as the diffusion operator in the plane orthogonal to the gradient of Q, that is,

$$\Delta_{\text{isod}}Q = \Delta_{\overrightarrow{\eta_1}}Q + \Delta_{\overrightarrow{\eta_2}}Q, \tag{1}$$

where $(\overrightarrow{\nabla Q}, \overrightarrow{\eta_1}, \overrightarrow{\eta_2})$ forms a normalized orthogonal reference system on each point of Ω.

Now let us give the analytical expression of the operator $\Delta_{\text{isod}}Q$. Using the fact that the Laplacian operator is invariant under rotation, and the fact that the reference system $(\overrightarrow{\nabla Q}, \overrightarrow{\eta_1}, \overrightarrow{\eta_2})$ could be obtained by rotating the canonical reference system (e_1, e_2, e_3), we have:

$$\Delta_{\overrightarrow{\eta_1}}Q + \Delta_{\overrightarrow{\eta_2}}Q + \Delta_{\vec{\zeta}}Q = \Delta Q, \tag{2}$$

where

$$\vec{\zeta} = \nabla Q.$$

Thus

$$\Delta_{\text{isod}}Q = \Delta_{\overrightarrow{\eta_1}}Q + \Delta_{\overrightarrow{\eta_2}}Q = \Delta Q - \Delta_{\vec{\zeta}}Q. \tag{3}$$

The expression of $\Delta_{\vec{\zeta}}Q$ is given by:

$$\Delta_{\vec{\zeta}}Q = \sum_{i,j=1}^{3} \lambda_{i,j}(Q)\partial_{x_i}\partial_{x_j}Q, \tag{4}$$

where:

$$\lambda_{i,j}(Q) = \frac{(\partial_{x_i}Q)(\partial_{x_j}Q)}{(\partial_{x_1}Q)^2 + (\partial_{x_2}Q)^2 + (\partial_{x_3}Q)^2}.$$

Let us now justify the link between the definition of ISOD operation and the iso-value surfaces. The following proposition proves that the orthogonal plane to the gradient is tangent to the iso-value surfaces.

Lemma 2.1. *Let f be a function defined on an open set Ω of $\Re^3$, and (x_0, y_0, z_0) a given point of Ω. We have the following result*: *$\nabla f(x_0, y_0, z_0)$ is orthogonal to the iso-values tangent plane defined by $f(x, y, z) = f(x_0, y_0, z_0)$ at the point (x_0, y_0, z_0).*

Proof. Let Σ be the iso-values surface defined by $f(x, y, z) = f(x_0, y_0, z_0)$. Assuming that $|\nabla f(x_0, y_0, z_0)| \neq 0$, then we can suppose that $\partial_{z_0} f \neq 0$ for instance. According to the implicit theorem functions, there exists a function $\varphi \in C^1$, defined on a neighborhood ϑ of (x_0, y_0), such that:

$$z = \varphi(x, y) \quad \forall (x, y) \in \vartheta$$

and the surface $(z, \varphi(x, y))$ belongs to Σ. One can verify that the vectors $v_1 = (1, 0, \partial_x\varphi(x_0, y_0))$, and $v_2 = (0, 1, \partial_y\varphi(x_0 y_0))$, generate the tangent plane to this surface at the point (x_0, y_0). On the other hand, the gradient of φ is given by:

$$\begin{pmatrix} \partial_x\varphi \\ \partial_y\varphi \end{pmatrix} = -(\partial_z f)^{-1} \begin{pmatrix} f_x \\ f_y \end{pmatrix}$$

and we obtain:

$$(1, 0, \partial_x\varphi) = (1, 0, -(\partial_z f)^{-1}\partial_x f)$$

and

$$(0, 1, \partial_y\varphi) = (0, 1, -(\partial_z f)^{-1}\partial_y f).$$

By computing the dot product, we verify that $(\partial_x f, \partial_y f, \partial_z f)$ is orthogonal to both v_1 and v_2, which completes the proof. □

This lemma proves that Δ_{isod} operator diffuses along the iso-values *only*. Now, let us see the local behavior of such viscosity. Consider a locally evolving iso-value surface (or curve) along a small time step of a given function that satisfies a diffusion equation with the ISOD operation. We propose to derive the diffusion model induced by the ISOD operator on the iso-values surfaces.

Proposition 2.1. *Let f be a function satisfying the iso-value oriented diffusion problem* (*i.e. a diffusion problem with ISOD as a diffusion operator*). *Thus, locally, the iso-values satisfy an anisotropic diffusion equation.*

Proof. For simplification purposes, the proof is carried out for the two-dimensional case. Let f be a function satisfying the ISOD diffusion problem, that is

$$\begin{cases} \partial_t f(t,x,y) - \Delta_{\mathrm{ISOD}} f = 0, & (t,x,y) \in [0,T] \times \Omega, \\ (0,x,y) = f_0(x,y), & f \in L^2(\Omega). \end{cases} \tag{5}$$

Let (t_0, x_0, y_0) a given point of $[0,T] \times \Omega$, there exists a function $\varphi(t,x)$ (implicit functions theorem) defined on a neighborhood ϑ of (t_0, x_0, y_0) such that

$$f(t,x,\varphi(t,x)) = f(t_0,x_0,y_0) \quad \forall (t,x) \in \vartheta.$$

The time and space derivatives are given by:

$$\partial_t \varphi = -\left(\frac{1}{\partial_y f}\right) \partial_t f \tag{6}$$

and

$$\partial_x \varphi = -\left(\frac{1}{\partial_y f}\right) \partial_x f. \tag{7}$$

Now we can compute the second derivative $\partial^2_{x^2} \varphi$:

$$\begin{aligned} \partial^2_{x^2} \varphi &= -\frac{\partial_y f \left[\partial^2_{x^2} f + \partial_{yx} f \partial_x \varphi\right] - \partial_x f \left[\partial_{xy} f + \partial^2_{y^2} f \partial_x \varphi\right]}{(\partial_y f)^2} \\ &= -\frac{\partial_y f \left[\partial^2_{x^2} f - \partial_{yx} f \frac{\partial_x f}{\partial_y f}\right] - \partial_x f \left[\partial_{xy} f - \partial^2_{y^2} f \frac{\partial_x f}{\partial_y f}\right]}{(\partial_y f)^2} \\ &= -\frac{1}{\partial_y f} \frac{\left[(\partial_y f)^2 \partial^2_{x^2} f - 2\partial_x f \partial_y f \partial_{xy} f + (\partial_x f)^2 \partial^2_{y^2} f\right]}{(\partial_y f)^2} \\ &= -\frac{1}{\partial_y f} \left(1 + \frac{(\partial_x f)^2}{(\partial_y f)^2}\right) \frac{\left[(\partial_y f)^2 \partial^2_{x^2} f - 2\partial_x f \partial_y f \partial_{xy} f + (\partial_x f)^2 \partial^2_{y^2} f\right]}{(\partial_x f)^2 + (\partial_y f)^2} \\ &= -\frac{1}{\partial_y f} \left(1 + \frac{(\partial_x f)^2}{(\partial_y f)^2}\right) (\Delta_{\mathrm{ISOD}} f). \end{aligned} \tag{8}$$

using (5)–(7) we obtain:

$$\partial^2_{x^2} \varphi = -\frac{1}{\partial_y f} \left(1 + (\partial_x \varphi)^2\right) \partial_t f,$$

and finally we achieve

$$\partial_t \varphi - \frac{1}{(1 + (\partial_x \varphi)^2)} \partial^2_{x^2} \varphi = 0.$$

We conclude that φ satisfies an anisotropic diffusion equation and that the diffusion is proportional to the inverse of the gradient. □

3. Application to FEM for Euler and Navier–Stokes equations

Here, we formulate the ISOD artificial viscosity for FEM in the case of the Navier–Stokes equations, the Euler equations being considered a subset.

Let the Navier–Stokes equations in conservative form be:

$$\partial_t U + \nabla.F(U) - \nabla.G(U,\nabla U) = S. \tag{9}$$

Consider these equations, with the ISOD artificial viscosity term added,

$$\partial_t U + \nabla.F(U) - \nabla.G(U,\nabla U) - \varepsilon\Delta_{\mathrm{ISOD}} U = S, \tag{10}$$

ε being a scalar viscosity coefficient that tends to zero. We do not emphasize the computation of this coefficient since it is not the goal of the paper. For the numerical tests we took the classical coefficient used for SU method.

To get a weak formulation of the ISOD operator for FEM that uses only shape functions of order one, some assumptions are needed. After a global reconstruction of the gradient, we consider a diffusion along the perpendicular plane to an average value of the gradient at each element. The transmission term between cells are neglected.

To proceed with the finite element discretization of the Navier–Stokes equations, a semi-discrete formulation and the classical corresponding approximation spaces are considered. Let ϑ_h be the trial solution space

$$\vartheta_h = \left\{ v/v(.,t) \in H^1(\Omega)^m, t \in [0,T],\ v/_{\Omega_e} \in P_k(\Omega^e)^m, v(.,t) = g \text{ on } \Gamma_g \right\} \tag{11}$$

and ω_h the weighting function space

$$\omega_h = \left\{ w/w(.,t) \in H^1(\Omega)^m, t \in [0,T],\ v/_{\Omega_e} \in P_k(\Omega^e)^m, w(.,t) = 0 \text{ on } \Gamma_g \right\}; \tag{12}$$

note that in our case $k = 1$.

The weak formulation of Eq. (6) is then given by:

Find $V \in \vartheta_h$

$$\underbrace{\int_\Omega (W.V_t - \nabla W.F(V) + \nabla W.G(V,\nabla V) + W.S)\,\mathrm{d}\Omega - \int_\Gamma W(-F(V) + G(V,\nabla V)).\vec{n}\,\mathrm{d}\Gamma}_{\text{NS term}}$$
$$+ \underbrace{\sum_e \int_{\Omega^e} \nabla W.(B^e \nabla V)\,\mathrm{d}\Omega - \int_{\partial\Omega^e\cap\Gamma} W(B^e V).\vec{n}\,\mathrm{d}\Gamma}_{\text{ISOD viscosityterm}} = 0 \quad \forall W \in \omega_h,$$

where

$$B_g^e = \varepsilon(I - A_g),$$

and

$$A_g(V) = \begin{pmatrix} \lambda_{1,1}(V) & \lambda_{1,2}(V) & \lambda_{1,3}(V) \\ \lambda_{2,1}(V) & \lambda_{2,2}(V) & \lambda_{2,3}(V) \\ \lambda_{3,1}(V) & \lambda_{3,2}(V) & \lambda_{3,3}(V) \end{pmatrix},$$

the subscript g designates the global reconstructed derivatives, as opposed to local derivatives.

In practice, we observe that by adding a term that diffuses in the direction of the gradient (similar to the discontinuities-capturing term introduced by Hughes [5] for SUPG) during just the first few iterations, the scheme becomes more robust. This is probably due to the simplifications we did to obtain a weak formulation using only P^1-elements, such a term is not needed if higher order shape functions are used. Consequently, the tensor B_g^ε is rewritten as:

$$B_g^\varepsilon = \varepsilon \left[(1-\alpha)(I - A_g) + \alpha A_g\right]. \tag{13}$$

The coefficient α is taken positive during just a few iterations and then set to zero.

Remark. For the FEM we used an implicit formulation, so the tensor $B_g^\varepsilon(V)$ is estimated at time step n when we compute for V^{n+1}. This linearization makes sense since we diffuse along the iso-values of the solution at a given time step to prevent oscillations of the next time step.

Lemma 3.1. *B^ε is a positive semi-definite matrix on Ω, $\forall \varepsilon$, $\alpha \geqslant 0$.*

Proof. To prove Lemma 3.1 it suffices to prove that both matrices A_g and $I - A_g$ are positive semi-definite. Noting that these matrices can be decomposed in the following manner:

$$A_g = A_1 A_1^t,$$

$$I - A_g = CC^t,$$

where

$$A_1(U) = \frac{1}{\sqrt{(\partial_x U)^2 + (\partial_y U)^2 + (\partial_z U)^2}} \begin{pmatrix} \partial_x U & 0 & 0 \\ \partial_y U & 0 & 0 \\ \partial_z U & 0 & 0 \end{pmatrix}$$

and

$$C(U) = \frac{1}{\sqrt{(\partial_x U)^2 + (\partial_y U)^2 + (\partial_z U)^2}} \begin{pmatrix} 0 & -\partial_y U & -\partial_z U \\ \partial_z U & \partial_x U & 0 \\ -\partial_y U & 0 & \partial_x U \end{pmatrix}.$$

This completes the proof. □

4. Numerical results

The proposed artificial viscosity is implemented, using the formulation developed in Section 3, in a 3D Euler/Navier–Stokes code, FENSAP (Finite Element Navier–Stokes Package). Here, we refer to each particular artificial viscosity model used in FENSAP as FENSAP-CU, FENSAP-SU, and FENSAP-ISOD, for classical upwind (CU), streamline upwind (SU), or ISOD, respectively.

First, let us see the behavior of the ISOD viscosity compared to the classical (CU) and streamlines (SU) upwind methods in the presence of numerical noise (non-physical oscillations due to the instability of the numerical method). In other words, examine the ability of each artificial viscosity to eliminate such noise without smearing shocks. Fig. 1 shows a noisy Euler solution over a NACA0012 at Mach = 0.85, at a 0° Angle of Attack (AoA). This solution is considered as the initial condition of a purely diffusive equation using the diffusion operator of each method. Taking the same amount of

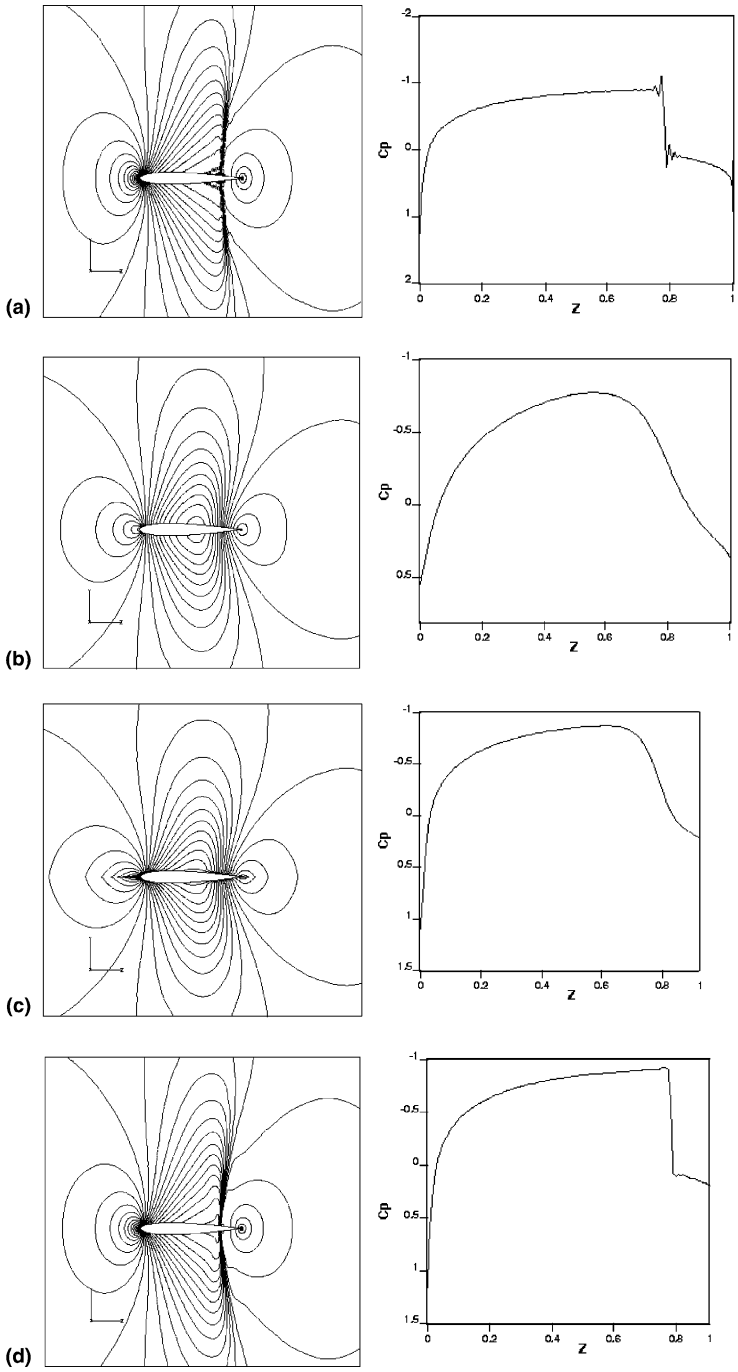

Fig. 1. Comparison of the diffusion effect around discontinuities between CU, SU, and ISOD method. (a) The initial data: Mach profile for inviscid transonic flow around NACA0012: Mach = 0.85, AoA = 0°, (b) diffusion solution for CU method, (c) diffusion solution for SU method, (d) diffusion solution for ISOD method.

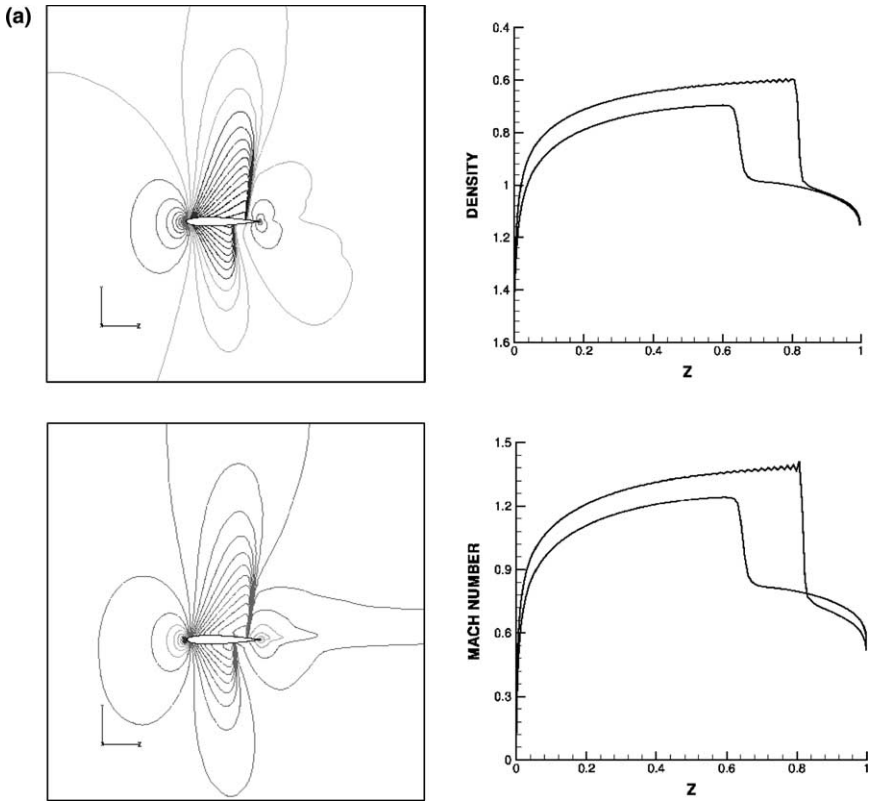

Fig. 2. Comparison of inviscid transonic flow around NACA0012 for the CU, SU, and ISOD methods. (a) Density and Mach solution for inviscid transonic flow around NACA0012: results using FENSAP-CU. Mach = 0.85, AoA = 1°, (b) density and Mach solution for inviscid transonic flow around NACA0012: results using FENSAP-SU. Mach = 0.85, AoA = 1°, (c) density and Mach solution for inviscid transonic flow around NACA0012: results using FENSAP-ISOD. Mach = 0.85, AoA = 1°, (d) Mach profile comparison: CU/ISOD and SU/ISOD.

viscosity, and after ten iterations in time, the figures show that the classical and streamline methods are highly diffusive (with less diffusion for the SU), removing the noise but with the shock quite smeared. The ISOD method shows, as expected, a greater ability to remove noise with a high quality of shock preservation, due to the diffusion over iso-surfaces that are parallel to the shock direction. In addition, note that for the classical rotating cone problem, the ISOD method is expected to give quite similar results to SU (or SUPG) methods since the streamlines are parallel to the iso-values lines for this test case.

Figs. 2(a)–(d) and 3(a)–(f) show, respectively, a 3D transonic Euler solution over a NACA0012 at Mach = 0.85, AoA = 1°, and a laminar supersonic solution around a NACA0012 at Mach = 2, AoA = 0° and Reynolds number = 500. The grids used are shown in the figures; a non-adapted grid with no grid clustering in the anticipated shock locations is used for the Euler solution, whereas an adapted grid is used for the laminar solution because it is somewhat difficult to get a good supersonic laminar solution on a coarse non-adapted mesh. Moreover, for all methods the coefficients proposed for SU (or SUPG) in [9] are used, multiplied by a coefficient ε that decreases to zero in order to get consistency at the limit. For the ISOD method the coefficient α is set to 0.5 at the beginning and decreased to zero after 50 iterations, by steps of 0.1. In Figs. 2(a)–(d), the density and Mach number profiles are shown, including the contours on

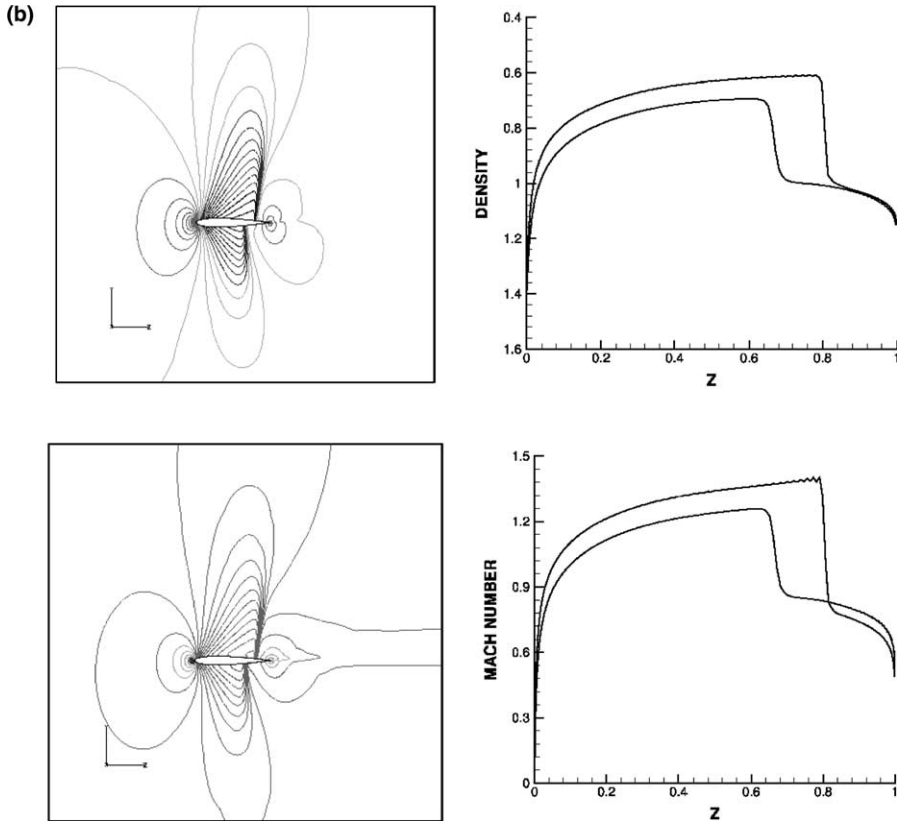

Fig. 2. (*continued*)

the wall (second figures on the right). One can appreciate the improved results when using the FENSAP-ISOD solver. Indeed, the noise in the FENSAP-CU and FENSAP-SU results is removed and the shock position is corrected. The density and Mach number are depicted in Figs. 3(a)–(f). It can again be noted that the results obtained with FENSAP-ISOD are noise-free and that the oblique shock is sharper and that the boundary layer is thinner.

In terms of CPU time, note that ISOD algorithm is a bit more complex than CU and SU algorithms since we need to compute the reconstructed gradient. However, and since solution features like shocks, expansion discontinuities and boundary layers are captured earlier, the steady state is reached within fewer iterations. Consequently, the ISOD CPU time is lower than other methods as shown in Table 1 for the transonic Euler test case described above. Note that the tests are run in parallel on a 4_CPU machine.

Since the use of ISOD helps in capturing discontinuities faster, Figs. 4(a)–(c) confirm the expectation that, for solutions that need mesh adaptation, the number of adaptation-solution cycles is sensibly reduced. The figures show the Mach profile of a supersonic flow on a NACA0012 wing at Mach 2, AoA $= 0°$ and Reynolds number $= 2000$. Good results are obtained after only 4 cycles of adaptation when using FENSAP-ISOD (Fig. 3(b)), while 7–9 cycles of adaptation are necessary to achieve comparable convergence with FENSAP-CU and FENSAP-SU (Fig. 3(c)).

Finally, in order to show that ISOD is suitable to a wide range of problems, we apply the method to two turbulent cases. The one-equation Spalart–Allmaras (S–A) model is selected first to predict the velocity profiles for turbulent flow over a flat-plate at $\mathrm{Re}_\theta = 10\,000$. The skin friction coefficient predicted

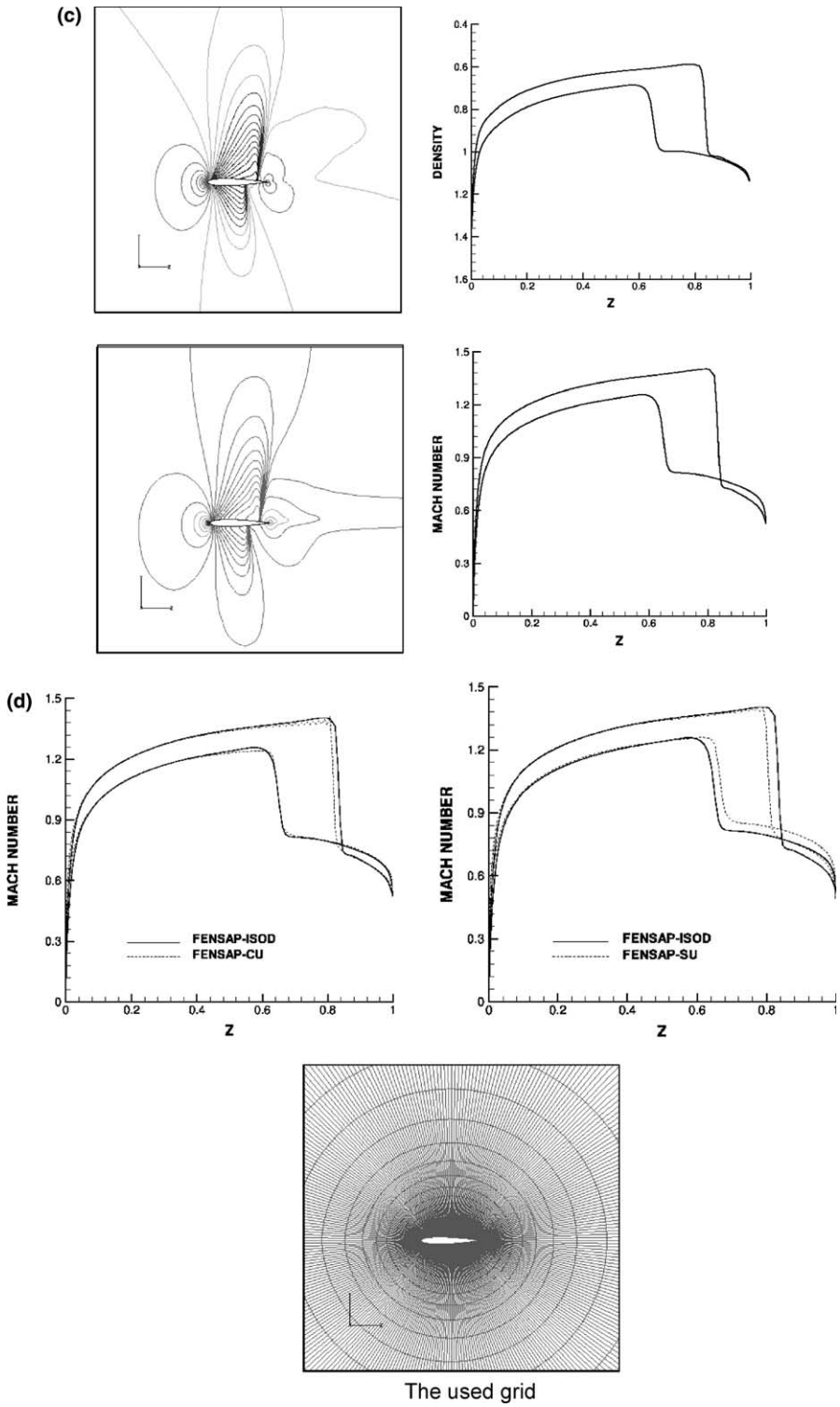

Fig. 2. (*continued*)

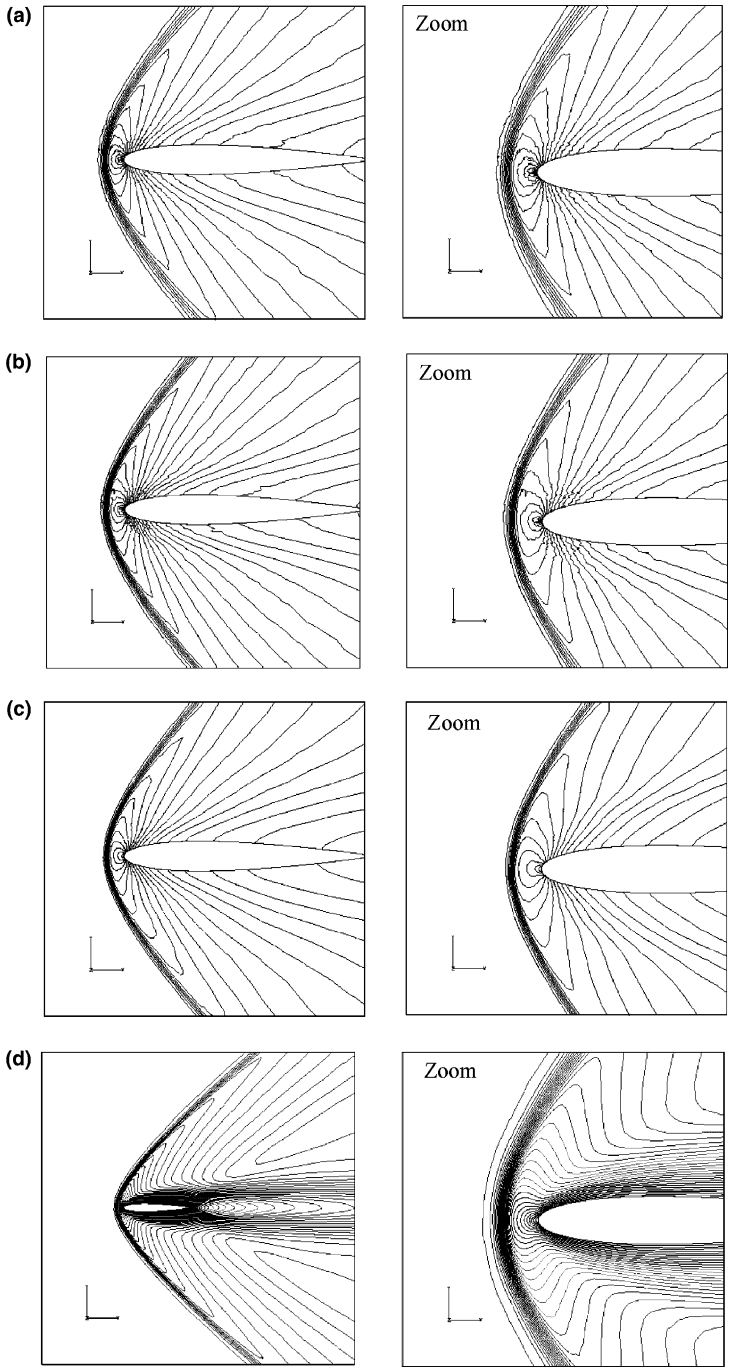

Fig. 3. Comparison for supersonic laminar flow around NACA0012 for the CU, SU, and ISOD methods. (a) Density profile of supersonic laminar flow around NACA0012; solution using FENSAP-CU, (b) density profile of supersonic laminar flow around NACA0012; Solution using FENSAP-SU, (c) density profile of supersonic laminar flow around NACA0012; solution using FENSAP-ISOD, (d) Mach profile of supersonic laminar flow around NACA0012; solution using FENSAP-CU, (e) Mach profile of supersonic laminar flow around NACA0012; Solution using FENSAP-SU, (f) Mach profile of supersonic laminar flow around NACA0012; Solution using FENSAP-ISOD.

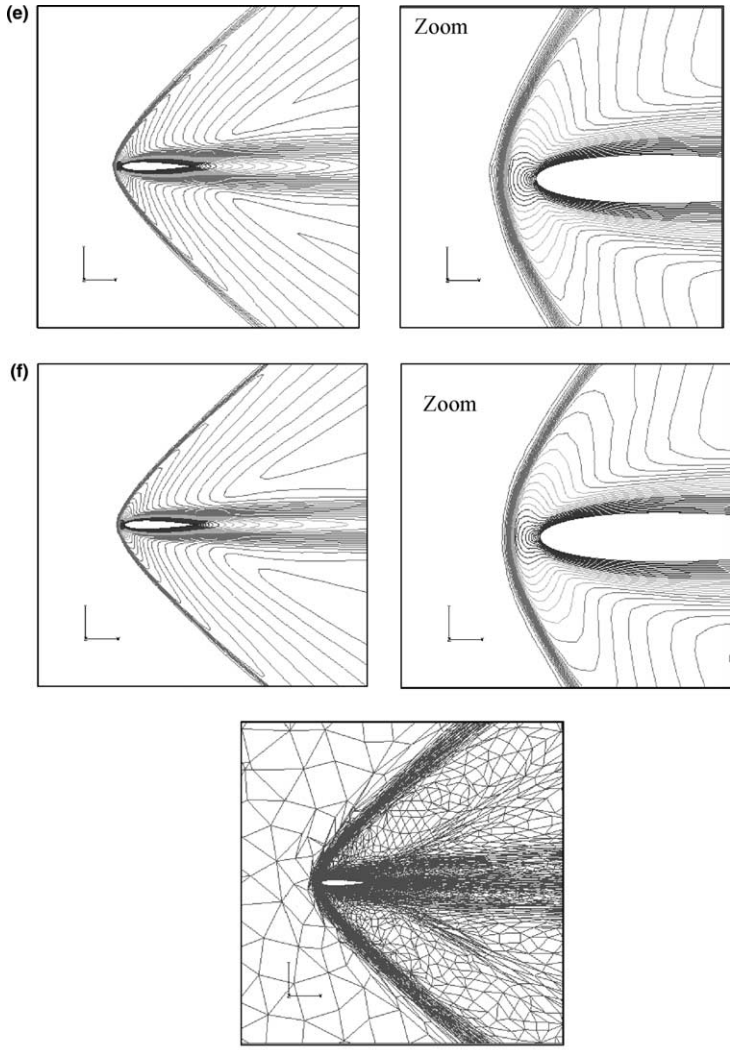

Fig. 3. (*continued*)

Table 1
CPU time and time-iteration number comparison for transonic Euler solution over a NACA0012 (Test case of Figs. 2a–d)

	CPU time/min	Number of iterations
FENAP-CU	19	300
FENAP-SU	17	250
FENAP-ISOD	14	200

with FENSAP-ISOD in this test case is $c_f = 0.00262$, which corresponds to the value adopted to calibrate the S–A model at $\mathrm{Re}_\theta = 10000$. The velocity profile in inner coordinates $u^+ = f(y^+)$ is shown in Fig. 5. The logarithmic curve clearly shows that the profile obtained agrees well with both measurements

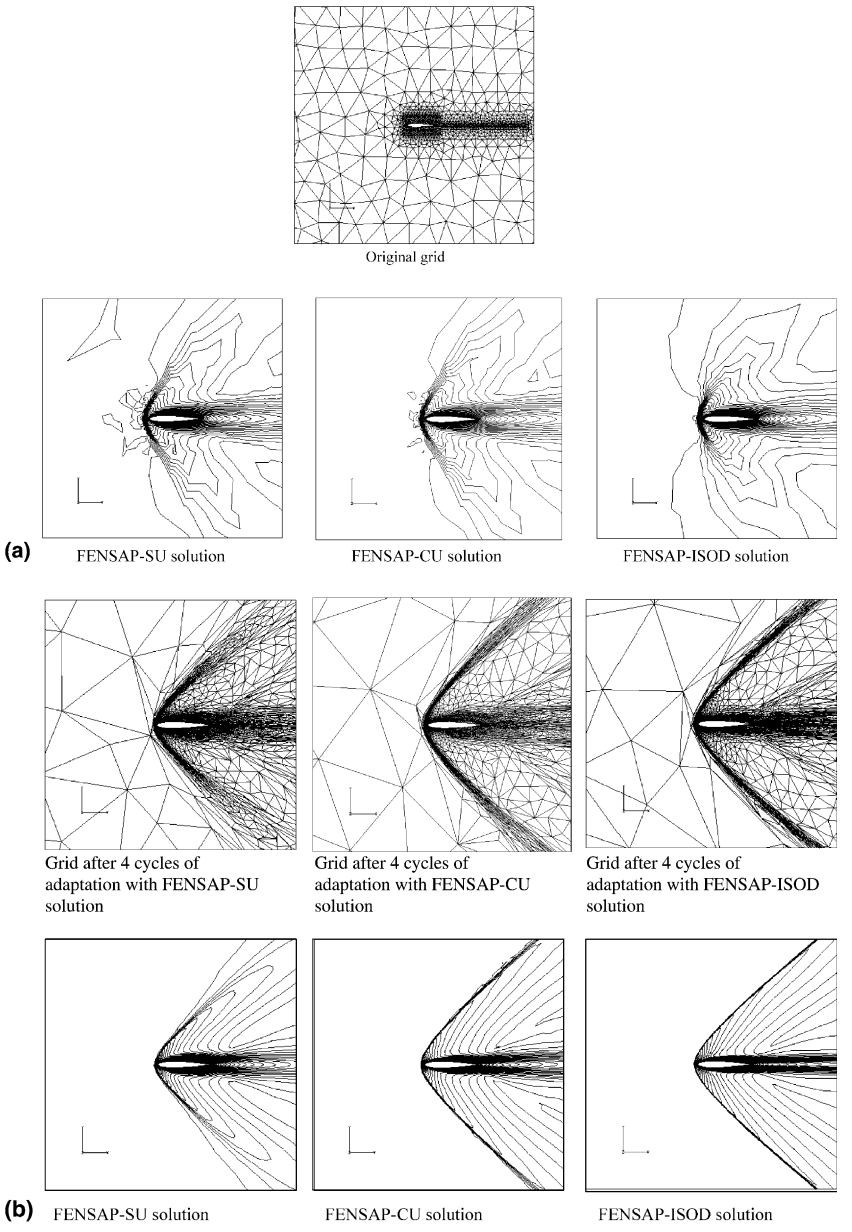

Fig. 4. (a) Mach solution on original grid: Mach $= 2.$, $\mathrm{Re} = 2000$, $\mathrm{A0A} = 0^0$, (b) Mach solution after 4 cycles of adaptations: $\mathrm{Mach} = 2.$, $\mathrm{Re} = 2000$, $\mathrm{A0A} = 0°$, (c) FENSAP-CU and FENSAP-SU Mach solutions after 7 and 9 cycles of adaptations, respectively. $\mathrm{Mach} = 2.$, $\mathrm{Re} = 2000$, $\mathrm{A0A} = 0°$.

[10] and the law of the wall. The second test case models a turbulent flow in a rough pipe. The velocity gradient near a rough pipe wall is less steep than that near a smooth one, as can been seen in Fig. 6, in which the velocity ratio u/U (U maximum velocity) obtained with FENSAP-ISOD using S–A has been plotted against the distance ratio y/R (R radius of the pipe) for a smooth and for several rough pipes. All

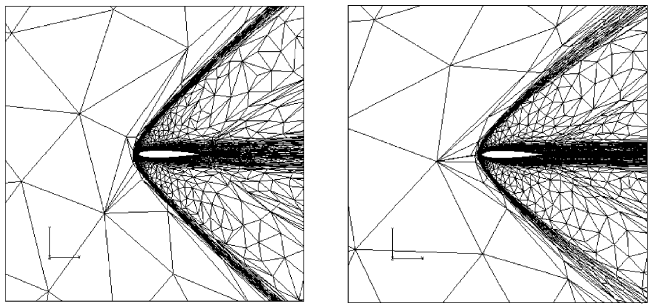

Grid after 7 cycles of adaptation with FENSAP-CU solution

Grid after 9 cycles of adaptation with FENSAP-SU solution

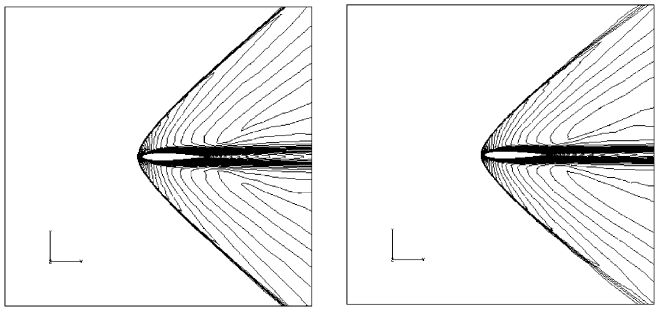

(c) FENSAP-CU after 7 adaptations

FENSAP-SU after 9 adaptations

Fig. 4 (*continued*)

have been compared to the measurements [11] and demonstrate the agreement of FENSAP-ISOD with experimental data.

5. Conclusions

We have proposed in this paper a new artificial viscosity model based on diffusion along the iso-values. This permits eliminating solution noise and ensuring stability without smearing discontinuities such as shocks. Some properties of the new method (referred to as ISOD) are formally derived and the efficiency of the method is shown through 3D numerical test cases for inviscid, laminar, and turbulent cases. A comparison with classical methods is also made. In addition to the improvement of the quality of the results, the proposed method also reduces the number of iterations necessary to reach the steady state as well as the number of cycles of mesh adaptation, if and when used.

Note that as viscous coefficients of the new method, we have used those proposed in the literature for SU (and SUPG) methods, scaled by a coefficient ε that decreases to zero during iterations to get consistency at the limit. As future work, it is planned to determine the optimal viscous coefficients for the proposed method. The use of higher order shape functions should also improve the accuracy and the robustness of the method through the estimation of the high order derivatives that were neglected in order to obtain the formulation of Section 3.

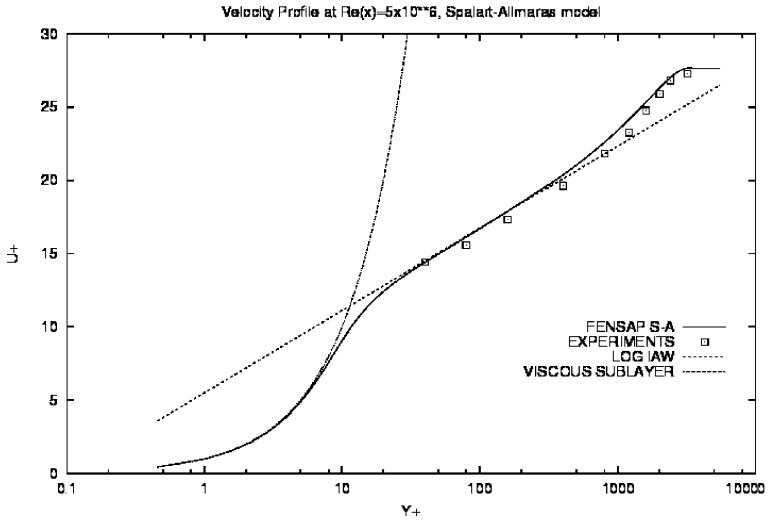

Fig. 5. Velocity profiles in a flat-plate boundary layer at $Re_\theta = 10000$ using FENSAP-ISOD on the Spalart–Allmaras one-equation model.

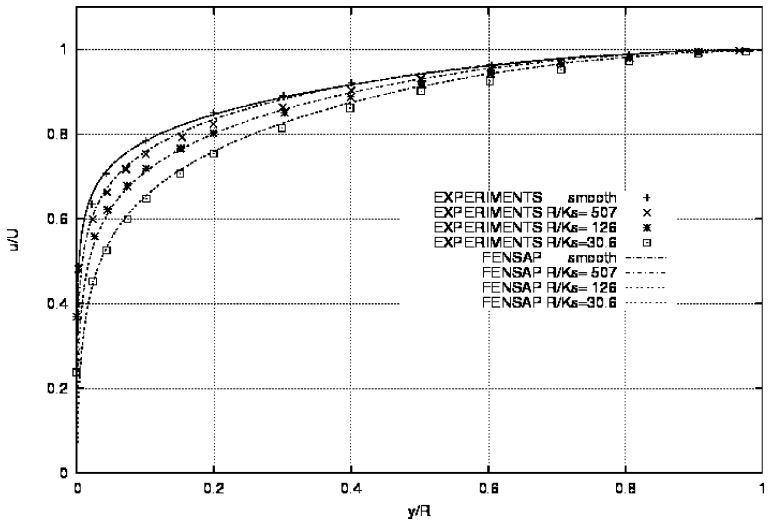

Fig. 6. Velocity profiles distribution in rough pipes, after Nikuradse [10].

References

[1] S.V. Patankar, in: W.J. Minkowycz, E.M. Sparrow (Eds.), Numerical Heat Transfer and Fluid Flow (Series in Computational Methods in Mechanics and Sciences), Hemisphere, Washington, 1980.
[2] O.C. Zienkiewicz, R.L. Taylor, The Finite Element Method, McGraw Hill, vol. I; 1989, vol. II, 1991.
[3] C. Hirsch, Numerical computations of Internal and External Flow, Wiley, vol. 1, 1988; vol. 2, 1990.
[4] S. Idelsoh, E. Onate, Finite element and finite volumes. Two good friends, Int. J. Numer. Methods Eng. 37 (1994) 3323–3341.
[5] E. Onate, S. Idelsohn, O.C. Zienkiewicz, R.L. Taylor, A finite point method in computational mechanics, application to convective transport and fluid flow, Int. J. Numer. Methods Eng. 39 (1966) 3839–3866.

[6] E. Onate, S. Idelsohn, O.C. Zienkiewicz, R.L. Taylor, C. Sacco, A stabilized finite point method for fluid mechanics, Comp. Methods Appl. Mech. Eng. 139 (1996) 316–346.
[7] A.J. Baker, Finite Element Computational Fluid Mechanics, Taylor and Francis, NY, 1983.
[8] J.C. Heinrich, P.S. Huyakorn, O.C. Zienkiewicz, A.R. Mitchell, "An upwind" finite element scheme for two-dimensional convective transport equation, Int. J. Num. Mech. Eng. 11 (1977) 131–143.
[9] A.N. Brooks, T.J.R. Hughes, Streamlines Upwind/Petrov-Galerkin formulation for convective dominated flows, with particular emphasis on the incompressible Navier–Stokes equations, Comput. Methods Appl. Mech. Eng. 32 (1982) 199–259.
[10] D.E. Coles, E.A. Hirst, Computation of Turbulent Boundary Layers-1968 AFOSR IFP-Stanford Conference, vol. II, Stanford Univ. Press, Stanford, CA, 1969.
[11] H. Schlichting, in: Boundary-Layer Theory, sixth ed., McGraw-Hill, New York, 1968, p. 581, Chapter 20.